THE EFFECT OF A HIGH THRUST PUSHER PROPELLER ON THE AERODYNAMIC CHARACTERISTICS OF A WING AT LOW REYNOLDS NUMBER

F.M. Catalano* and J.L. Stollery**
College of Aeronautics
Cranfield, Bedford, England.

Abstract

An experimental and theoretical study was performed in order to investigate the effects of a high thrust pusher propeller on the aerodynamic characteristics of a two-dimensional wing. The scope of the experimental study was to test several different positions of propeller and wing and to measure effects on the wing characteristics. Measurements included surface pressure distributions, lift, drag, pitching moment, and boundary layer behaviour by flow visualisation. A semi-inverse viscous computer program which includes the propeller inflow velocities was developed in order to predict the propeller effects on the wing. It is shown that the inflow suction from the propeller affects a large part of the wing and it is clearly dependent on the wing/propeller position. When testing a smooth wing the transition was moved downstream with a related increase of the laminar part of the boundary layer. Theoretical predictions showed good agreement with the experimental results through the range of incidence tested.

Nomenclature

a	propeller inflow factor
$b_{1/2}$	half the width at half depth in turbulent jet theory
c	wing chord
C_T	thrust coefficient
C_D	drag coefficient
C_L	lift coefficient
C_{Lmax}	maximum lift coefficient
$C_{mc/4}$	quarter chord pitching moment coefficient
J	advance ratio
L'	laminar separation point
R	reattachment point
R_l	slipstream radius of a isolated propeller
Rd_i	local displaced slipstream radius
R_p	propeller radius
R_{llo}	slipstream radius at the lower surface
R_{lu}	slipstream radius at the upper surface
RHS_i	right hand side vector of panel *i*
S	separation point
S_f	frontal area of the wing immersed in the slipstream
T	transition point
U_{si}, W_{si}	axial and vertical velocities induced by the wake sinks at panel *i*
V_{ni}	transpiration velocity at panel *i*
V_∞	free stream velocity
V_{px}, V_{pz}	axial and vertical velocities induced by the propeller inflow
Vt_i	tangential velocity at panel *i*
Xp, Zp	axial and vertical distances from the propeller
α	model incidence angle
θ	panel inclination
σ	free constant in turbulent jet flow
χ	free constant
ε_v	virtual kinematic viscosity

* PhD, LAE/EESC-USP Brazil, Member AIAA
** Professor, College of Aeronautics, England, Fellow AIAA.

Introduction

A large number of flight vehicles have been developed to operate at chord Reynolds numbers less than 500,000. Among these vehicles are high-altitude remotely piloted vehicles[1]; low-altitude[2-3], low-velocity mini-RPVs and ultralight recreation aircraft. Most of these aircraft use a propeller in the pusher configuration Recent work[4-5] on the propeller-wing interaction have shown potential benefits in fuel efficiency and cabin noise from using an advanced propeller in pusher configuration.. As there is little effect of the propeller inflow on the aerodynamic characteristics of the wing in a large aircraft, interest focuses on the interference of the wing and pylon wakes on the propeller efficiency, vibration and noise. However, for general aviation and RPVs the distance between the wing and the pusher propeller can be close enough to induce quite large effects on the wing surfaces, especially when the propellers are operating at high thrust as in take-off and climb. The new composite technologies and structural design have allowed the construction of high aspect ratio wings which means that the propeller inflow will have considerably effect not only on the rear part of the wing, but also on the front part because of the small wing chord. At take-off the aircraft speed is close to the stall velocity and the whole process, involves a large range of incidences with the propeller operating all the time at maximum thrust. Therefore, the velocities induced by the propeller inflow on the wing in this situation, will also be of considerably magnitude when compared with the wing's flowfield velocities. Much experimental and theoretical work has been done on the effect of a pusher propeller on the wing, notably by Maunsell[6] and Jonhson & White[7] . However, Maunsell[6] carried out the tests at just one incidence and the theory did not included viscous calculations. While Jonhson[6] carried out tests at a wide range of model incidence but the propeller/wing positions were limited to the over the wing configuration and no theoretical calculations were developed. In Ref. 8, the effects of the over the wing propeller were estimated by using a panel method program with the propeller flow approximated by a nacelle with control face to determine the mass flow. The propeller inflow was well simulated but again, no viscous calculations were carried out. The present research concentrated on testing the effect of a high thrust pusher on a two-dimentional wing at a wide range of incidences and with the propeller positioned at several different positions behind the wing (Fig.4). In order to predict more accurately the wing's flowfield, a semi-inverse computer programme[9] was used in conjunction with Koning's propeller theory[10] in a similar approach to that used by Maunsell[6].

Experimental Arrangement

A Wortmann FX63-137 profile wing with a chord of 0.34m was used for the tests. The wing carried 82 pressure tapping around the centre-line chord. A 0.52 m diameter three blade propeller driven by a 20 hp hydraulic motor was used. The propeller geometry is shown in Fig. 1. Thrust was measured using a special strain-gauge balance and the rotational speed by a pulse meter. For the pressure measurements the College of Aeronautics' 8x4 ft open return low-speed wind tunnel was used with the wing positioned vertically in the working section (Fig. 2). The propeller was mounted on a separate pylon which could be moved in order to set the propeller/wing positions. The wing could be moved vertically through the working section in order to measure the spanwise effect of the propeller on the surface pressure distribution. The force and moment measurements were made in the CoA 8x6 ft closed-circuit low-speed wind tunnel using a similar arrangement to that described above. The wing was attached vertically to a six-component balance and spanned the tunnel except for a 3mm gap at one end so that force measurements could be made (Fig. 3). Flow visualisation was carried out using both sublimation and oil techniques.

Range of Tests

Seven wing/propeller positions (Fig.4) were tested through the incidence range of -4 to +20 degrees for the wing, with and without a trip wire. Wing surface pressure distributions were taken at 10 spanwise positions. The Reynolds number was set at 0.45 millions and the propeller was run at a thrust coefficient of $C_T=0.15$ with an advance ratio of $J=0.33$. These propeller characteristics were chosen in order to simulate a high power condition such as take-off or climb.

Theory

Full details of the computational programme used for the calculations of the aerodynamic characteristics of the wing are given in the paper by Williams[9]. The programme uses an integral boundary layer method which has been extended to calculating separated flow by assuming a two parameter description of the separated velocity profiles. The programme is of the semi-inverse type in which a direct inviscid calculation is coupled to an inverse calculation of the boundary layer. The outer inviscid flow is assumed here to be both incompressible and irrotational, so that it can be described by the relevant solution of the Laplace's equation, which is obtained by a surface singularity method. In the inner viscous flow, the laminar portion of the boundary layer is calculated by Thwaites's, and natural transition is predicted using Granville's correlation. If laminar separation occurs before transition, then the laminar separation bubble is calculated using Horton's semi-empirical technique. The development of the turbulent boundary layer and wake is calculated by the inverse formulation of Green's lag-entrainment method. The axial and vertical velocities induced by the propeller inflow inside the slipstream given by Koning's theory were included in the inviscid calculations of the programme, and in the global panel coordinates of the programme, there are given by:

$$V_{P_x} = a\left(1+\frac{X_p}{\sqrt{(R_p/c)^2+X_p^2}}\right) \tag{1}$$

$$V_{P_z} = -\frac{1}{2}a\frac{(R_p/c)^2 Z_p}{\sqrt{\left((R_p/c)^2+Z_p^2\right)^3}} \tag{2}$$

where:

$$a = \frac{1}{2}\left(-1+\sqrt{1+\frac{8}{\pi}\frac{C_T}{J^2}}\right) \tag{3}$$

Because the simplifications in Koning's theory, Vp_x and Vp_z are constant inside the slipstream in a plane normal to the X and Z axis respectively with a discontinuity between the inside and the outside flow of the slipstream. In the flow upstream of a propeller, this discontinuity is not present because a process of mixing smooths out the transition in a similar way to that found in turbulent jets and wakes. In order to find a practical solution for the problem, it was assumed that the propeller inflow will behave as a "reversed" turbulent jet flow with a maximum velocity at the centre of the jet given by equations (1) and (2). Thus, the equations for turbulent jet[11] could be adapted, and after a coordinate transfer to the global panel coordinates there were given by:

$$Vp_{x,z} = (Vp_{x,z})_{Koning}(1 - \tanh^2\eta) \tag{4}$$

where

$$\eta = \sigma\frac{Y}{X} \quad with \quad \sigma = \frac{1}{2}\sqrt{\frac{Vp_{x,z}X}{\varepsilon_\tau}} \tag{5}$$

The virtual kinematic viscosity ε_τ is a function of the width of the jet and the central line velocity and is given by:

$$\varepsilon_\tau = \chi b_{1/2}(Vp_{x,z})_{Koning} \tag{6}$$

The free constant χ was determined experimentally following the methodology of Schlichting[11]. The width of the jet was assumed equal to the slipstream radius at the wing surfaces and wake. The slipstream radius was calculated based on the fact that by continuity the volume flowing through the slipstream must remain the same for both isolated propeller and for a propeller with a wing in front, so that we have:

$$\pi R d_1^2{}_i - S_{f_i} = \pi R_1^2{}_i \tag{7}$$

$$with \quad S_{f_i} = \frac{1}{2}t_i\left(2R_{1u_i} + 2R_{1w_i}\right) \tag{8}$$

$$R_{1u_i} = \sqrt{R_1^2 - (Z_p - t_{u_i})^2} \tag{9}$$

$$R_{llo_i} = \sqrt{R_1^2 - (Z_p - t_{lo_i})^2} \qquad (10)$$

Where $t_i = t_{ui} + t_{loi}$ is the local airfoil thickness and R_{lu} and R_{llo} are functions of the propeller vertical position Z_p. Equation (7) is a polynomial equation in Rd_l from which only the real and positive root was taken in order to find the slipstream boundary geometry. The best value found for χ was 0.3 and some results can be seen in Fig. 05. Without the propeller effects the ***RHS*** vector of the system of equations which calculates the strength of the unknowns is formed by the normal components of V_∞ and the normal velocities from the wake sinks and vortices for the inviscid solution plus the transpiration velocity from the viscous calculation. With the propeller effects, the ***RHS*** vector becomes:

$$(RHS_i)_{on} = (RHS_i)_{off} + VP_{x_i} Sin\theta_i + VP_{z_i} Cos\theta_i \qquad (11)$$

And the tangential velocity at the control point of the panel i determined after the system reaches a satisfactory convergency is given by:

$$(Vt_i)_{on} = (Vt_i)_{off} + VP_{x_i} Cos\theta_i + VP_{z_i} Sin\theta_i \qquad (12)$$

The two-dimensional calculations were carried out at strips in the spanwise direction and the results were integrated through the span in order to obtain the overall effect of the propeller inflow on the wing.

Results and Discussion

All the experimental results were corrected for model blockage. The propeller thrust, and the advance ratio were corrected for blockage using Glauert's[11] methodology. Corrections were made for the interference effects of the nacelle and pylon (propeller off) on the wing ahead. Fig. 6 shows the pressure distribution at the centre line of the wing at various incidence angles. Fig. 7 shows the spanwise normal force coefficient distribution calculated from integration of the pressure distributions. At low incidence, with a trip wire fitted, the turbulent boundary layer does not separate so that the effect of the propeller inflow velocities is mainly a change of the flow incidences angles and an increase of the momentum over both upper and lower surfaces. Hence the main effects of the propeller inflow on the wing at low incidence are an increase in lift and an increase in the pressure drag of the wing.

The main effect of the propeller inflow on the wing at high incidence angle is on the turbulent separation of the boundary layer on the upper surface. For all the propeller positions the effect of the propeller inflow, changing flow incidence and increasing velocities, delayed turbulent separation. Flow visualisation tests revealed that the turbulent separation point along the centre line can be moved downstream by up to 56%c from the separation point for the propeller-off case. The evident benefit of these effects is a decrease in pressure drag due to separation and a delay of the stall of the wing. For propeller positions above the chord line of the wing (positions 02, 03, 04, and 05), the circulation and consequently the lift of the wing increases when compared with the positions on the chord line (positions 01 and 06). This is due to the bigger amount of momentum injected into the flow over the upper surface of the wing. When above the chord line, the propeller inflow also acts directly on the upwash in front of the wing increasing the local flow incidence. In the spanwise direction, the effect of moving the propeller above the chord line is to reduce the wing area affected by the propeller inflow due to the inflow slipstream constriction. This slipstream constriction induces a cross flow velocity which affects significantly the rear section of the wing for propeller positions near the trailing edge of the wing. Therefore, for positions above the wing chord line, the beneficial effect of the propeller inflow on the turbulent separation position decreases more rapidly in the spanwise direction, due to the constriction of the inflow slipstream of the propeller. The combination of the normal and cross flow components of the propeller induced velocity can promote early separation at the slipstream boundaries on the wing upper surface.

Fig. 8 shows the pressure distribution at the centre line for the wing with smooth surfaces. All the effects of the propeller inflow on the wing pointed out above, are also valid for the case of a smooth wing. However, the process of transition from a laminar to a turbulent boundary layer on a smooth wing at this Reynolds number is likely to be completely different from that on the wing with a trip wire, and the propeller inflow can affect this process. At low incidence, there is generally a formation of a laminar separation bubble followed by transition to a turbulent shear layer, and reattachment. As the incidence increases, the bubble contracts and moves upstream. This mechanism was found at most of the incidences tested and the approximate positions of laminar separation, transition and reattachment are shown in the pressure distributions by the letters L', T and R respectively. Fig. 9 shows the results of the flow visualisation tests with the propeller off and on at positions 01 and 03, using the sublimation technique for finding transition, and oil flow for determining of the turbulent separation. The most significant effect of the propeller inflow on the upper surface is that the position of transition has moved downstream. This is shown in Fig. 8 by the movement downstream of the pressure distribution kink between X/C=0.6 and X/C=0.8. This means that laminar boundary layer flow was extended by the effect of the propeller inflow. Flow visualisation tests also shown that inside the propeller inflow slipstream there was a slight increase of the bubble length with a maximum at the centre of the wing aligned with the propeller longitudinal axis. The flow visualisation tests also showed that there was no measurable effect of the propeller inflow on the transition from laminar to turbulent flow for $\alpha \geq 8°$, as can be seen in Fig. 9.

Fig. 10 shows the C_L-α, C_D - C_L, $C_{Mc/4}$ and L/D-C_L curves for positions 01 to 07 for the wing with the trip wire. Fig. 10 shows the increase in C_{Lmax} due to the effect of the propeller inflow on turbulent separation. The increase on the drag of the wing at low and middle incidence and with the propeller on, is produced mainly by the increase of the pressure drag. The main benefit of the propeller inflow on the wing can be seen from the C_L - C_D polar plots, with the propeller on, the working range of C_L of the wing is considerably increased.

From the L/D-C_L curves it is evident that the effect on the pressure drag due to the propeller inflow, led to an overall improvement on the aerodynamic characteristics of the wing only for propeller position above the wing. For all the propeller positions there was a decrease in the magnitude of C_M. Because the propeller inflow changes the stall of the wing, the slight increase in the magnitude of C_M observed after the stall for the propeller off case (typically at $\alpha = 12°$) virtually disappeared for most of the propeller positions. There was no evidence that the aerodynamic centre of the wing changes significantly.

Fig. 11 shows the C_L-α, C_D - C_L, $C_{Mc/4}$ and L/D-C_L curves for positions 01, 02, 03 and 07 for the smooth wing. As expected the best improvements on the C_L-α characteristics were obtained for propeller positions above the wing. The rapid lift loss at $\alpha = 18°$ and $\alpha = 20°$ for the wing with the propeller off, disappeared with the propeller on for all the propeller positions tested. The increase in the total drag at incidences between $\alpha = 8°$ and $\alpha = 16°$ was mainly due to an increase in the pressure drag.

Fig. 12 shows the effect of the advance ratio on the lift and drag of the wing. As expected, significant changes in the lift and drag only occur for advance ratios lower than 1. The effect of moving the propeller to different positions downstream of the trailing edge and keeping the same vertical distance from the chord line, can be seen in Fig. 13. By extrapolation it can be predicted that after d/c = 1.5 the increase on C_L will be virtually zero. The same behaviour can be expected for the effect of the propeller inflow on the drag and pitching moment values. From these results it is evident that in order to have a large effect on the wing, the propeller must be placed close to the trailing edge and be operating at high thrust.

Fig. 14 shows the comparison of the experimental pressure distribution results with the theory for α=7.5°, position 01 and the wing with trip-wire. The results are quite good for most of the spanwise stations despite the discrepancies at the peak of suction due to the presence of the trip wire. Fig. 15 shows that the lift coefficient calculated by integrating the theoretical pressure distribution in the spanwise direction can satisfactorily predict the effect of the propeller inflow on the wing. The theoretical results agree well with the pressure distribution for the wing with smooth surfaces, as can be seen in Fig. 16. Transition and turbulent separation on the smooth wing can also be predicted by the theory as shown in Fig. 17. The theoretical method for this Reynolds number, always gives transition by means of a laminar separation bubble whereas in the experiment the transition is natural between $\alpha = 6°$ and $\alpha = 14°$.

Conclusions

The effect of a high thrust pusher propeller on the aerodynamic characteristics of a straight wing was investigated by wind tunnel tests and predicted by a semi-inverse computer programme coupled with the analytical propeller theory of Koning[10]. A total of seven different positions between propeller and wing were investigated for the wing with and without a trip wire.

The propeller induced flow over the wing surfaces, thus increasing the lift, increasing pressure drag and delaying turbulent separation. The extent of attached flow was increased substantially with the propeller operating. The effect of the propeller inflow was more intense on the rear part of the wing, but can also extend to the front by changing the upwash angle. Pitching moment was also increased by the propeller inflow although no change of the aerodynamic centre was verified. The propeller inflow can also delay transition by preserving laminar flow in a smooth wing operating at low Reynolds number thus causing a reduction in the skin friction drag.

The propeller inflow effects are very dependent on the propeller/wing relative position. Over the working range of incidences the propeller positions above the wing gave the best results. The propeller effect will be small if the propeller is positioned more than one propeller diameter behind the wing.

The Williams[9] semi-inverse computer programme in conjunction with Koning's theory gave good results for the centre line pressure distribution. The spanwise effect of the propeller inflow simulated by adapting the turbulent jet flow equations also gave good agreement with the experimental results. The flow over wings in a pusher configuration operating at low Reynolds, can also be well predicted despite the difficulties with the transition point calculations.

References

1- **Langford, J.S.:** - New Aircraft Platforms for Earth System Science an Opportunity for the 1990s. ICAS-90 5.8.1 pp 1534-1538 Vol 2.

2- **Siddiqi S. and Kwa T.:** The Design and Flight Testing of a Long Endurance RPV. ICAS-90-5.8.2.

3- **Stollery, J.L. and Dyer D.J.:** Wing-Section Effect on the Flight Performance of a Remotely Piloted Vehicle. Journal of Aircraft, Vol 26, NO. 10 1989.

4- **Goldsmith, I.M.:** A Study to Define the Research and Technology Requirements for Advanced Turbo/Propfan Transport Aircraft. NASA CR-166138, 1981.

5- **Dunham, D.M.; Gentry, G.L., Jr.; Gregory M.S.; Applin, Z.T.; and Quinto P.F.:** Low Speed Aerodynamic Characteristics of a Twin-Engine General Aviation Configuration wiyh Aft-Fuselage-Mounted Pusher Propellers. NASA TP-2763, 1987.

6- **Maunsell, M.G.:** A Study of Propeller-Wing-Body Interference for a Low Speed Twin-Engined Pusher Configuration. ICAS-90-5.4.3, 1990.

7- **Johnson J.L. and White E.R.:** Exploratory Low Speed Wind Tunnel Investigation of Advanced Commuter Configurations including an Over-the-Wing propeller design. AIAA-83-2531, 1983.

8- **Cooper R.K.; McCann W.J. and Chapleo A.Q.:** Over Wing Propeller Aerodynamics. ICAS-92-3.2.2, 1992.

9- **Williams B.R.:** The Prediction of Separated Flow Using a Viscous-Inviscid Iteraction Method, R.A.E. Tech. Memo. Aero 2010, Farnboroug, Dec. 1984.

10- **Koning C.:** Influence of the propeller on the Other Parts of the Airplane Structure. Div. M Aerodynamic Theory, Vol. IV, Edited by Durand W., C.I.T. Cal. 1935.

11- **Schlichting H.:** Boundary Layer Theory, McGraw-Hill, Inc, 1979.

12- **Glauert H.:** The Elements of Aerofoil and Airscrew Theory, second edition, Cambridge University Press 1947.

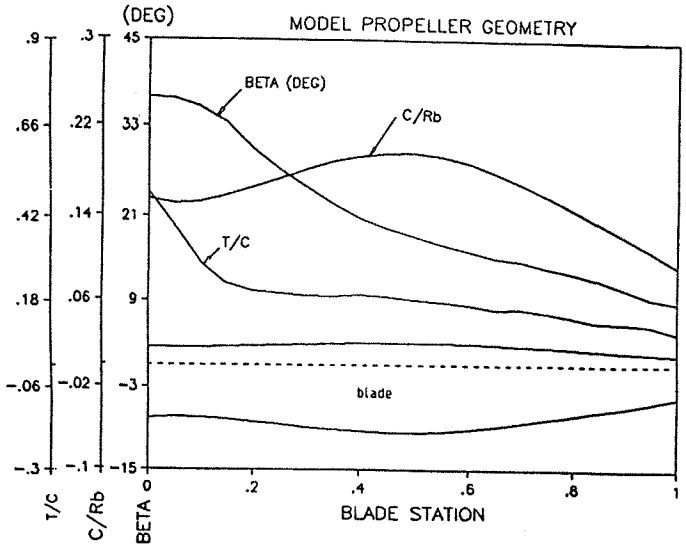

Fig. 1 Model Propeller geometry

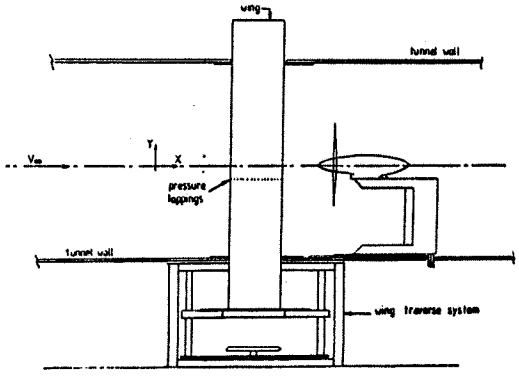

Fig. 2 Experimental set-up for pressure distribution measurements.

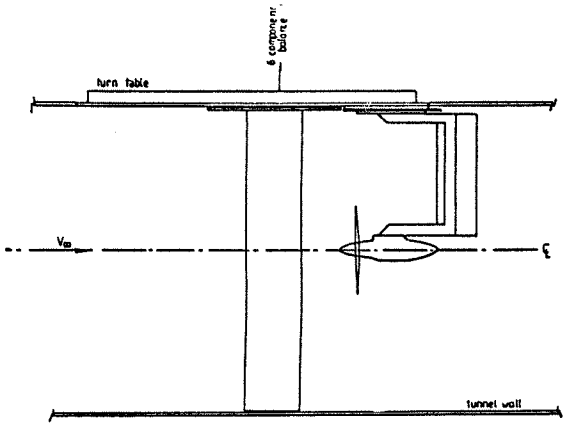

Fig. 3 Experimental set-up for forces and moment measurements.

PROPELLER POSITION	Xp	Zp
POS 01	0.5c	0.0
POS 02	0.5c	0.23c
POS 03	0.5c	0.46c
POS 04	0.85c	0.46c
POS 05	0.85c	0.23c
POS 06	0.85c	0.0
POS 07	0.5c	-0.19c

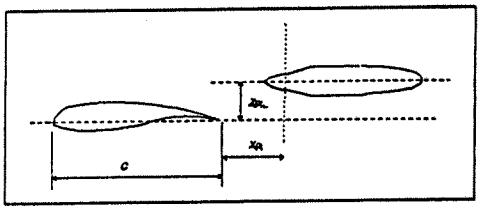

Fig. 4 Propeller positions.

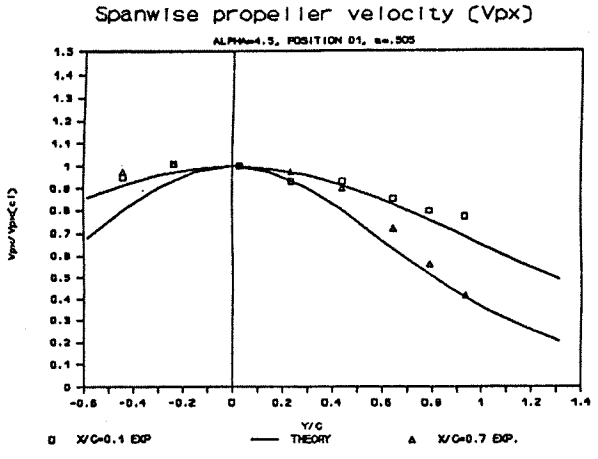

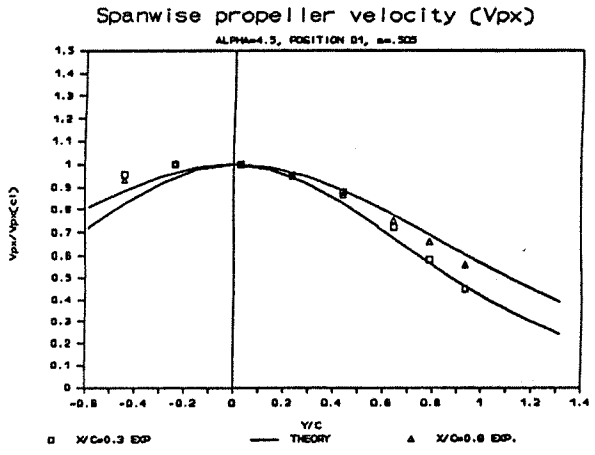

Fig. 5 Equation (4) with $\chi = 0.3$ for propeller position 01

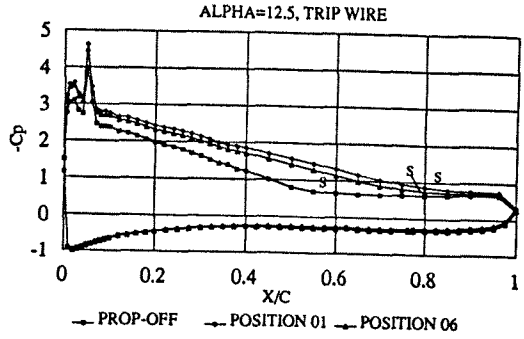

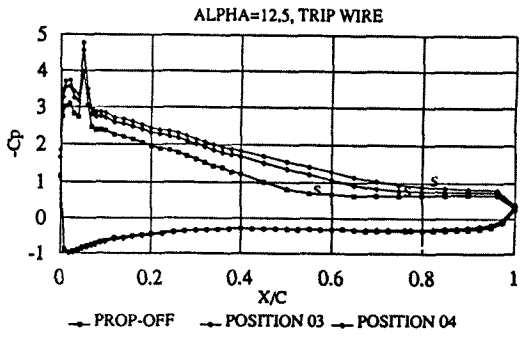

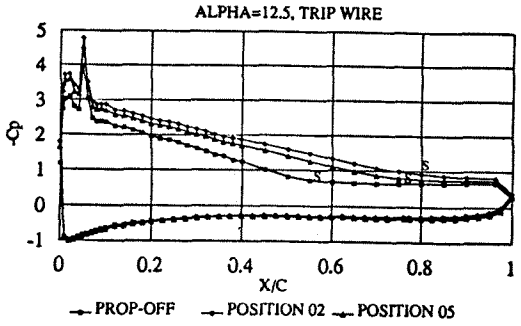

Fig. 6 Pressure distribution at the centre line, all propeller positions and $\alpha = 12.5°$.

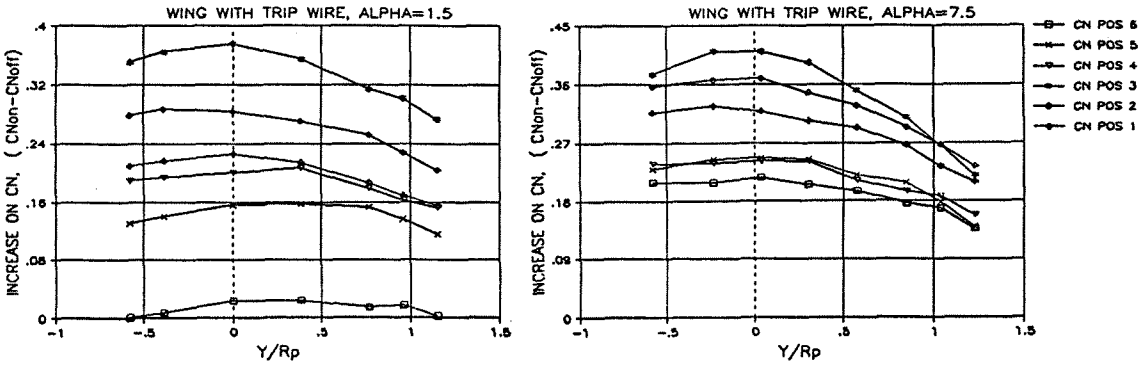

Fig. 7 Spanwise normal force coefficient, by integrated pressure distributions.

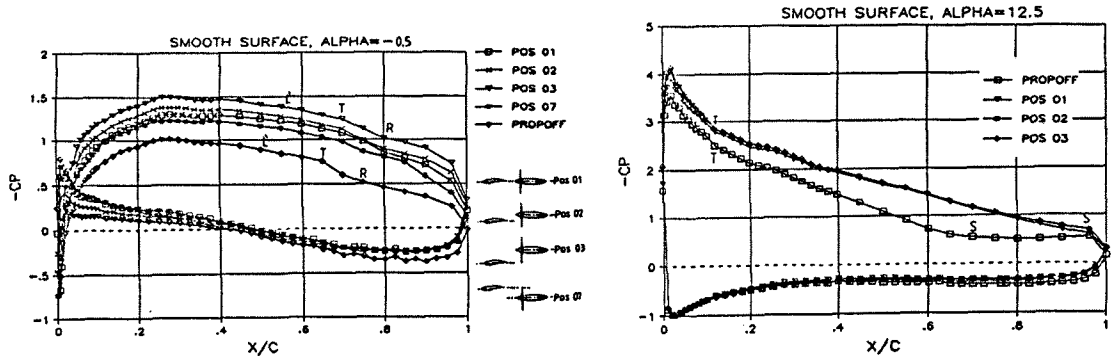

Fig. 8 Pressure distribution at the centre line for the smooth wing.

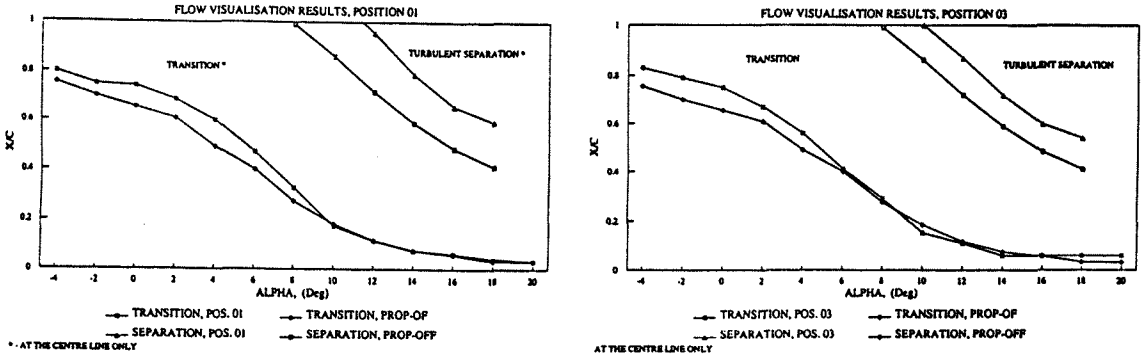

Fig. 9 Transition and separation from flow visualisation tests, positions 01 and 03.

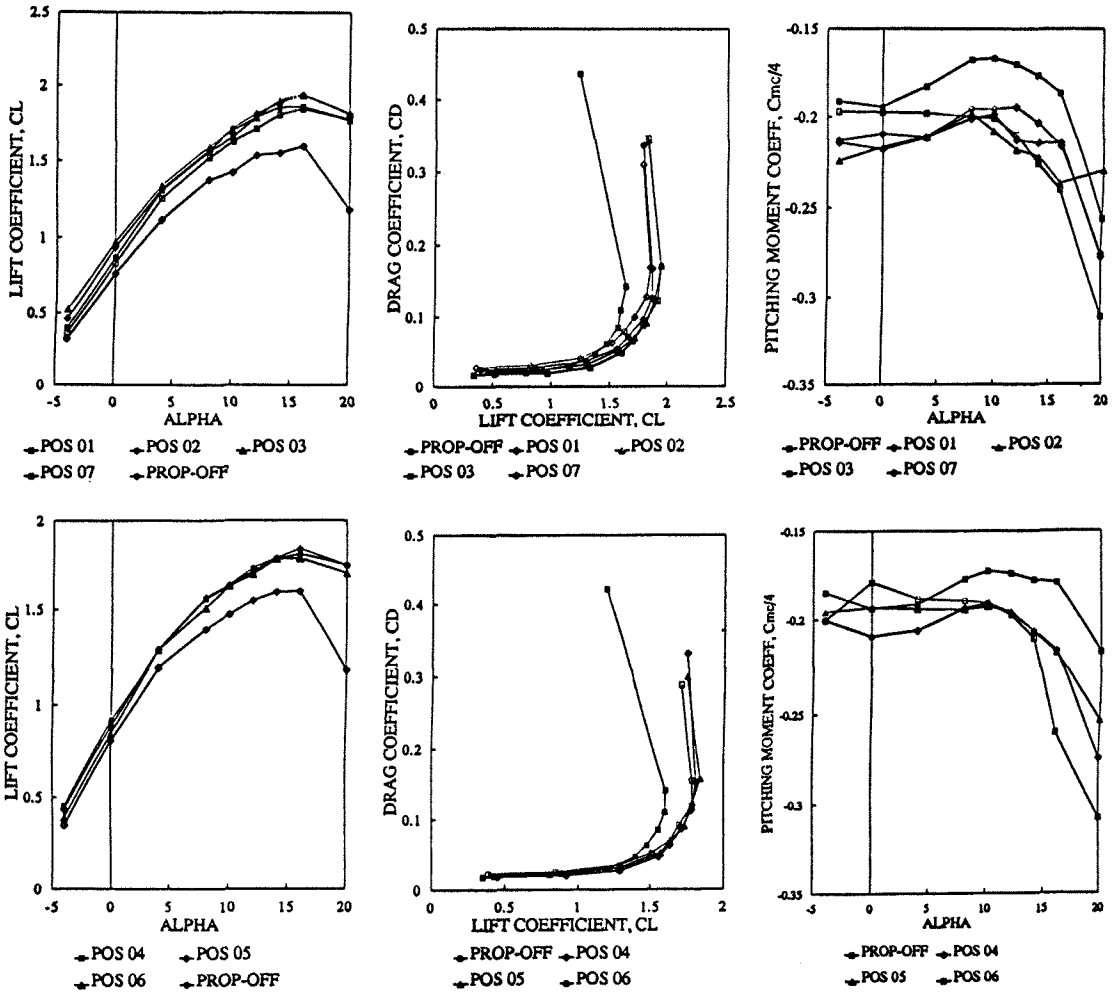

Fig. 10 Lift, Drag and pitching moment for the wing with trip wire.

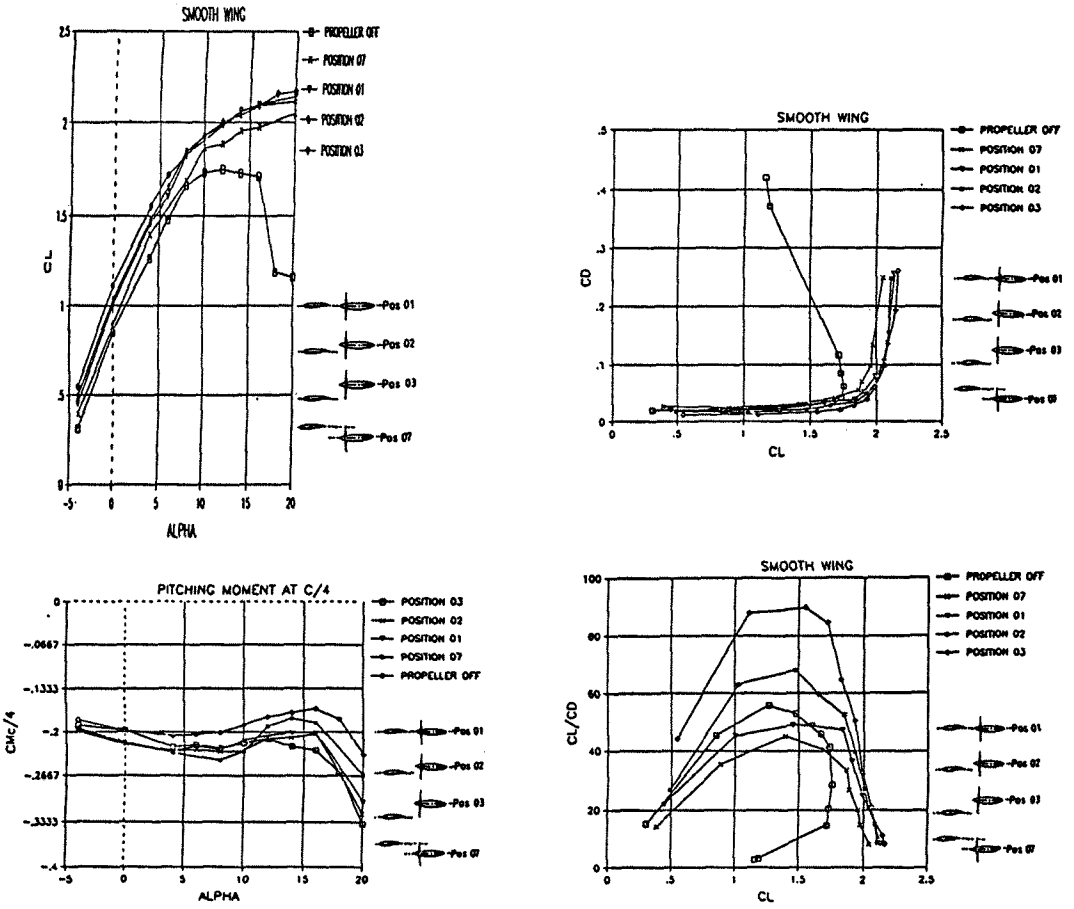

Fig. 11 Lift, Drag and pitching moment for the smooth wing.

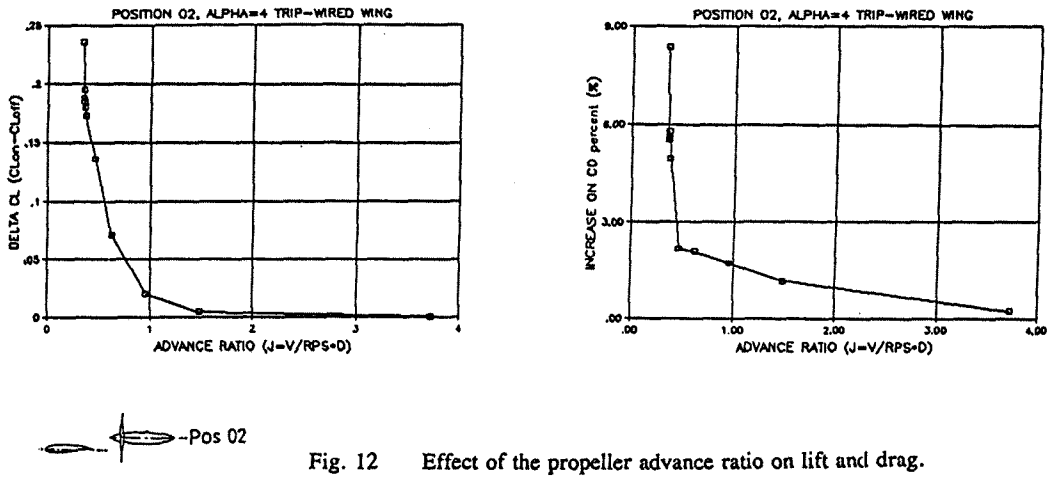

Fig. 12 Effect of the propeller advance ratio on lift and drag.

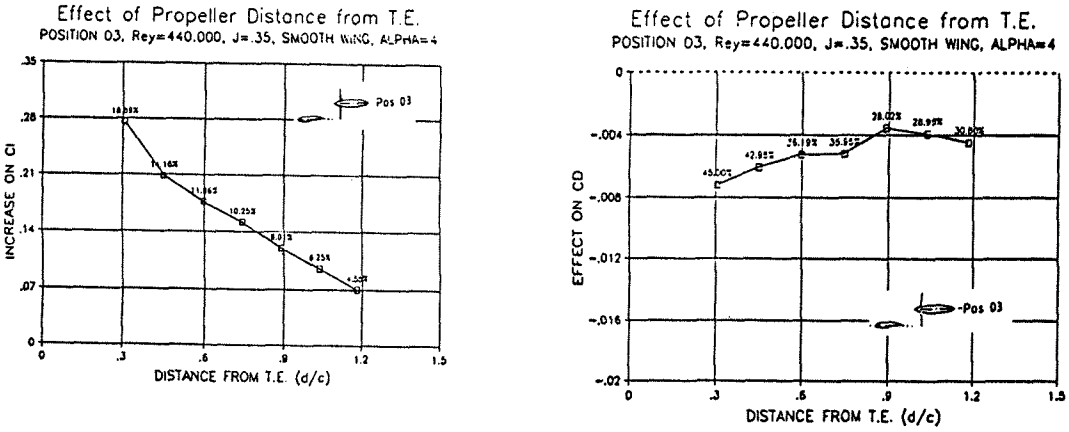

Fig. 13 The effect of moving the propeller to positions downstream the wing.

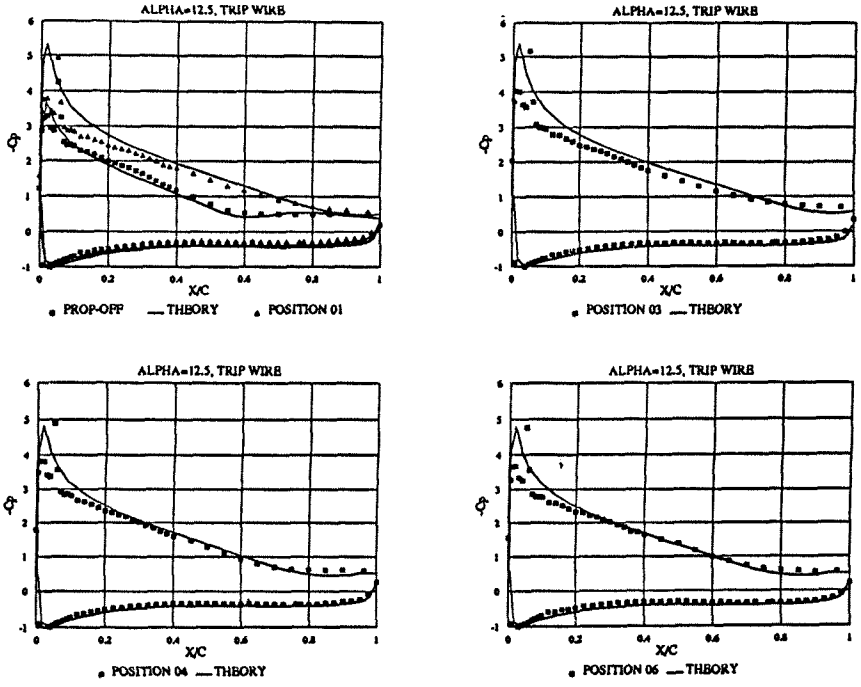

Fig. 14 Comparison with theory, centre line pressure distributions, trip-wired wing, propeller positions 01, 03, 04 and 06, $\alpha = 12.5°$.

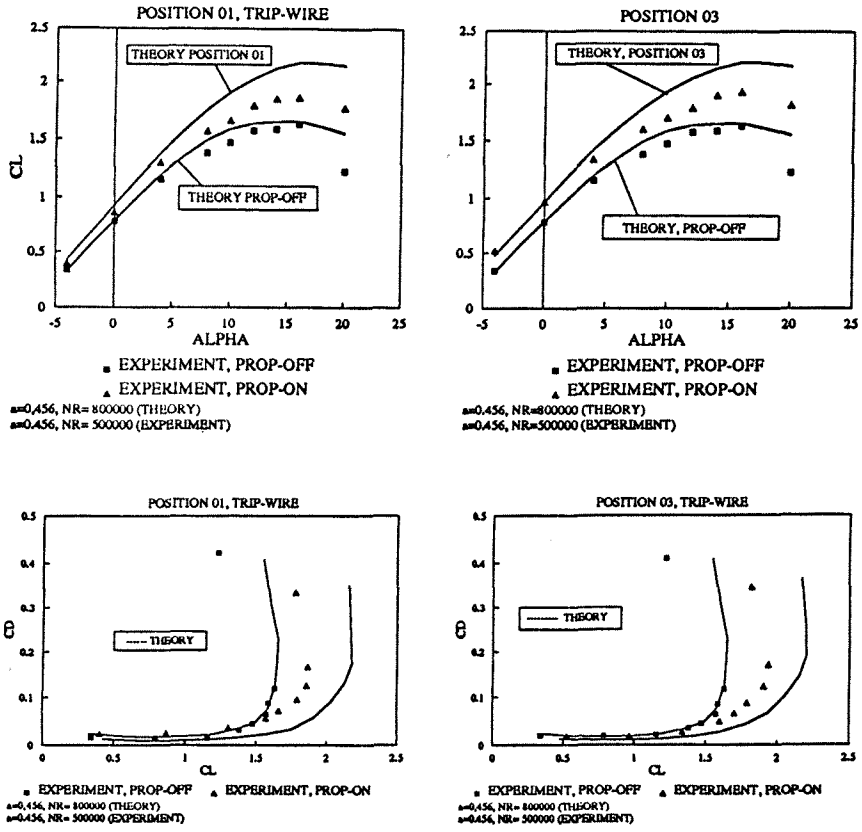

Fig. 15 Comparison with theory, integrated spanwise distribution of calculated C_L and C_D, trip-wired wing, propeller position 01.

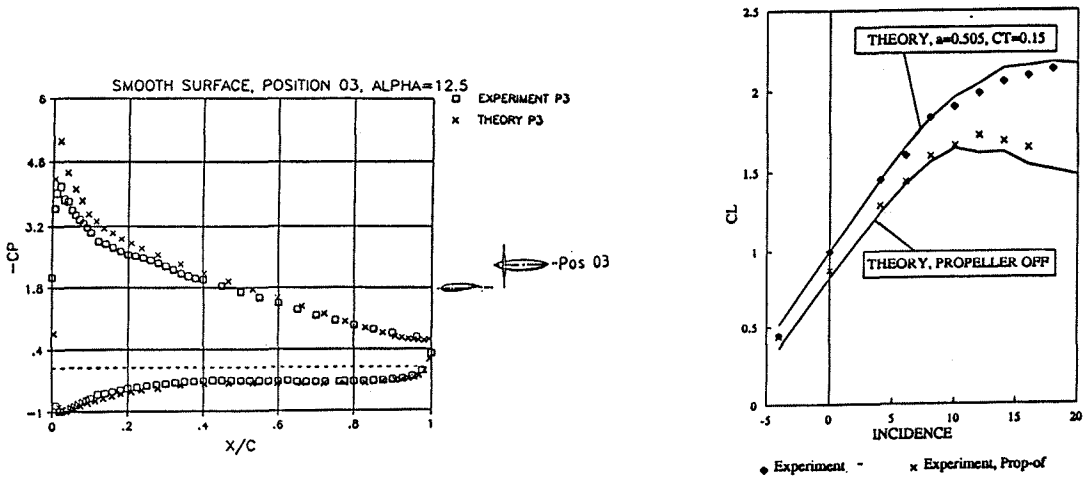

Fig. 16a Comparison with theory, smooth wing.

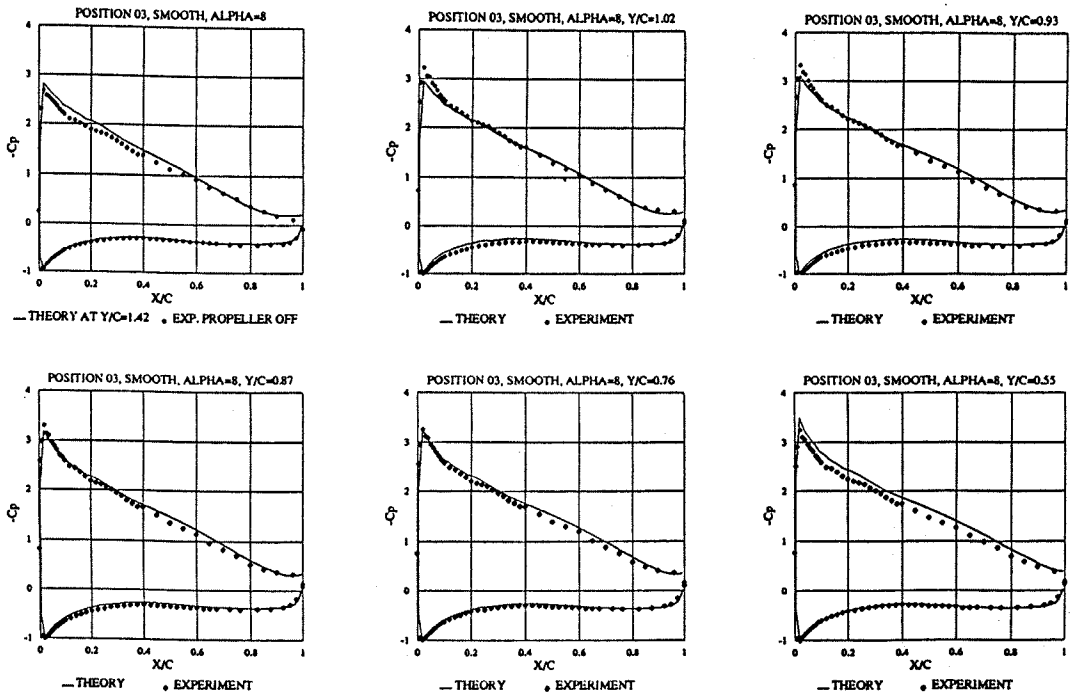

Fig. 16 b Comparison with theory, smooth wing.

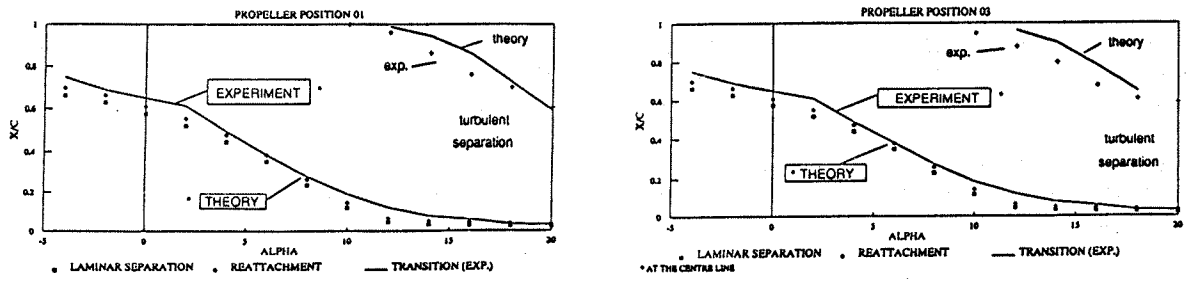

Fig. 17 Comparison with theory, transition and turbulent separation.